Electrochimica Acta 219 (2016) 742–750

Contents lists available at ScienceDirect

Electrochimica Acta

journal homepage: www.elsevier.com/locate/electacta

A high-performance flexible solid-state supercapacitor based on Li-ion intercalation into tunnel-structure iron sulfide

Muhammad Sufyan Javed[a,b,1], Zhiqiang Jiang[a,1], Cuiling Zhang[a], Lin Chen[a], Chenguo Hu[a,*], Xiao Gu[a,*]

[a] Department of Applied Physics, Chongqing University, Chongqing 400044, PR China
[b] Department of Physics, COMSATS Institute of Information Technology, Lahore 54000, Pakistan

ARTICLE INFO

Article history:
Received 6 June 2016
Received in revised form 10 October 2016
Accepted 10 October 2016
Available online 12 October 2016

Keywords:
Iron sulfide
tunnels
intercalation
nanospheres
pseudocapacitor

ABSTRACT

A flexible solid-state supercapacitor based on iron sulfide (FeS_2) nanospheres supported on carbon-paper is fabricated, which exhibits excellent electrochemical performance such as, high capacitance of 484 F g^{-1} at a scan rate of 5 m Vs^{-1}, good rate capability, and excellent cycling stability (95.7% after 5000 cycles). The supercapacitor achieves high energy density of 44 Wh kg^{-1} at power density of 175 W kg^{-1} with high coulombic efficiency (97%). Three charged supercapacitors connected in series can power 12 green-color light-emitting-diodes (LED, 3.0 V, 20 mA) for 5.5 minutes. To understand the detailed electrochemistry, we have carried out both experimental and theoretical investigations. The pseudocapacitive characteristics of the FeS_2 nanospheres are systematically investigated by a single electrode in aqueous electrolyte. According to our structural analysis, the FeS_2 nanospheres have orthorhombic structure, where Fe atoms are surrounded by 6 S atoms to form a FeS_6 octahedron. These octahedrons are connected to form a network structure, which provide tunnels (2.55 × 4.77 Å). With all the evidence, we believe that the FeS_2 nanospheres could be a promising material for supercapacitor electrodes.

1. Introduction

Among the various energy storage devices, supercapacitors (SCs) are considered as one of the most important green energy storage devices with advantages of high power density, good operational safety and long life span [1,2]. Nanostructure electrode materials provide better accommodation of strains during ion intercalation/de-intercalation in Faradaic process, which enhances the performance of supercapacitors. Additionally, porous or nano-network structure would increase electrode-electrolyte contacting area and promote ion diffusion [3]. These effects surely improve rate capability and capacity of various materials, leading to better performance of supercapacitors. Therefore, developing nanostructured electrode materials with superior electrochemical performance is highly desirable. Recently, nanostructured transition metal chalcogenides (TMCs) have attracted more attention as a new class of electrode material for supercapacitors. TMCs have achieved better performance comparing with the carbon or transition metal oxides (TMOs) based materials [4,5]. Experimental investigations have revealed that the redox reactions among different valence states of metal ions in TMCs are similar to the transition metal oxides (TMOs) [4–6]. The mixed-valence chalcogenides are of significance as most of them exhibit interesting electrical or magnetic properties, such as metallic conductivity [7,8] and superconductivity [9]. As the size of S^{2-} and Se^{2-} is larger than that of O^{2-}, the polarization of anion framework is larger; this benefits the mobility of cations in overcoming deformation from the ion intercalation. The other advantage is the higher charge negativity of the anion framework, which can enhance the cation density and promote ion conductivity. There are many reports on the supercapacitors based on different types of TMCs, such as copper sulfide [4], nickel sulfide [10], zinc sulfide [11], cobalt sulfide [12], molybdenum sulfide [13] and nickel-cobalt sulfide [14] and so on. Wan et al. reported hydrothermal synthesis of cobalt sulfide (CoS) nanotubes, which exhibits a specific capacitance of 285 F g^{-1} in 6 M KOH aqueous electrolyte [12]. Dai et al. reported hydrothermal synthesis of C/KCu_7S_4 wires based symmetric SC, which shows excellent electrochemical performance with specific capacitance of 469 mF cm^{-2} in LiCl-PVA solid electrolyte [15]. Ratha et al. reported hydrothermal synthesis of layered tungsten disulfide/reduced graphene oxide

* Corresponding authors. Tel.: +86 23 65670880; fax: +86 23 65678362.
E-mail addresses: hucg@cqu.edu.cn (C. Hu), gx@cqu.edu.cn (X. Gu).
[1] These authors contributed equally to this work.

http://dx.doi.org/10.1016/j.electacta.2016.10.060
0013-4686/

composite, which exhibits a high capacitance of 350 F g^{-1} in 1 M of Na_2SO_4 aqueous electrolyte [16].

Among different crystal structures, layered and tunnel structures would be the best option for high performance pseudocapacitors [8,17] and have recently attracted much attention. These structures provide efficient pathways for ions insertion or extraction, which enhance total charge storage of electrodes [9]. Electrode materials with tunnel structures such as α, β-MnO_2 [18], Mn_3O_2 [19] and KCu_7S_4 [17] have one-dimensional tunnels and exhibit excellent electrochemical charge storage performance. Similarly, iron sulfide (FeS_2) possesses a network structure by FeS_6 octahedrons. In orthorhombic FeS_2, Fe atom is surrounded by 6 S atoms to form FeS_6 octahedron, and these FeS_6 octahedrons are connected to form network structure. Such network structure of the octahedrons could provide fast electron transmission and the tunnels along c direction with cross-section size could offer diffusion paths for the ion intercalation/de-intercalation during the charging/discharging process [20]. Therefore, it should be an interesting work to investigate the supercapacitor behaviors of the nanostructured iron sulfide.

In this study, the iron sulfide nanospheres (FeS_2) assembled by nanoparticles are synthesized by the hydrothermal method. The FeS_2 nanospheres supported on carbon paper (CP) exhibits the large specific capacitance of 852.3 F g^{-1} in LiCl liquid electrolyte at a scan rate of 10 m Vs^{-1} with excellent stability. The FeS_2-CP is directly served as binder free electrode in symmetric flexible solid-state supercapacitors. The FeS_2-CP solid-state supercapacitor exhibits large specific capacitance of 484 F g^{-1} at scan rate of 5 m Vs^{-1} with good stability. A maximum energy density of 44 Wh/kg at a power density of 175 W/kg is attained with 97% of coulomb efficiency. Three supercapacitors connected in series can charged up to 3 V and power 12 green color light-emitting-diodes (3.0 V, 20 mA) effectively for 5.5 minutes. This work indicates that the FeS_2 is promising material for supercapacitors due to the specific tunnel structure of FeS_2 and the nanoparticle aggregated spheres.

2. Experimental and calculation

2.1. Synthesis of FeS_2 nanospheres

The FeS_2 nanospheres is synthesized by simple hydrothermal process, in a typical experiment, 2 mmol of iron nitrate hydrate ($Fe(No_3)_3{\cdot}9H_2O$) was first mixed in 20 mL of distilled water under constant stirring for 10 min to get a clear solution. Then 1 mL of ethylenediamine (EN) was added into the solution drop-wise and the solution turned to dark red under stirring for 30 min. Finally, 1 mL of carbon disulfide (CS_2) was introduced into the above solution as a sulfur source and further stirred for another 30 min. After that, the solution was transferred into a Teflon-lined stainless autoclave of 50 mL capacity and then Teflon autoclave was put into 200 °C preheated furnace for 24 hours. After completing reaction, the autoclave was cool down to room temperature naturally and the precipitates were washed with ethanol and deionized water. The final product was dried in an electric oven at 60 °C for 6 hours. The schematic demonstration of the synthesis process for the FeS_2 nanospheres is illustrated in Fig. S1A.

2.2. Preparation of single electrode and all-solid-state-supercapacitors

Carbon paper (CP) and all other chemicals were purchased from Aladdin and used without any further processing. CP is used as a substrate for the fabrication of single electrode and all-solid-state supercapacitor. The as-prepared FeS_2-nanospheres were deposited into a piece of CP (2 cm^2) by vacuum filtration pump and dried at 60 °C. In the fabrication process of all-solid-state supercapacitor; first, the CP was cut into pieces of 4 × 2 cm^2 and FeS_2 nanospheres were deposited on the pieces of CP using a simple vacuum filtration pump and dried for 1 hour at 65 °C. The active mass of FeS_2 nanosphere on the CP was approximately 1.0 mg cm^{-2}, carefully weighted by an electronic balance before and after the deposition. The two pieces of FeS_2-nanospheres coated CPs were face-to-face sandwiched with a separator and thin layer of LiCl-PVA solid electrolyte. The PVA-LiCl electrolyte has a thick layer of 0.45 mm in in supercapacitor device and its ionic conductivity is 0.15 S cm^{-1}. PVA-LiCl gel electrolyte was simply prepared as follow: 12.6 g LiCl was mixed with 60 mL deionized water and then 6 g PVA powder was added. The whole mixture was heated to 85 °C under vigorous stirring until the solution becomes clear. The schematic demonstration of the fabrication method of flexible all-solid-state supercapacitor based on the FeS_2-CP is shown in Fig. S1B.

2.3. Material Characterizations

The crystallographic structure of the as-prepared FeS_2-nanospheres was characterized by X-ray powder diffraction (XRD) (PANalyticalX'Pert Powder, Cu Kα radiation). The surface morphology of the FeS_2 product was investigated by field emission scanning electron microscope (FEI Nova 400 FEG-SEM) and a transmission electron microscope (TEM, TECNAI20 Philips). The BET surface area was calculated using the multipoint Brunauer-Emmett-Teller (BET) method at 77.0 K with a quantachrome (NOVA4200e). The Nitrogen absorption and desorption isotherms were used to investigate the pore size distribution by Barrett–Joyner–Halenda (BJH).

2.4. Electrochemical Measurements

The cyclic voltammetric analysis (CV) and galvanostatic charge-discharge (GCD) measurements were conducted using an electrochemical workstation (CHI 660D). The electrochemical impedance spectroscopy (EIS) measurements were carried out at open circuit potential in the frequency range of 100 m Hz to100 kHz. The electrochemical performance of FeS_2-nanospheres based electrode was investigated using three electrode system in 1 M LiCl liquid electrolyte. The as-fabricated FeS_2-CPs, platinum foil and saturated calomel electrode were used as working electrode, counter electrode and reference electrode, respectively.

2.5. Theoretical calculation

In order to investigate the possible Li^+ intercalations in orthorhombic FeS_2, first principles calculations based on density functional theory (DFT) were carried out. All calculations are accomplished using a plane wave basis set and the projector augmented wave (PAW) method as implemented in the Vienna Ab initio Simulation Package (VASP) [17]. The Perdew-Burke-Ernzerhof (PBE) of the spin-polarized generalized gradient approximation (GGA) was used for the exchange-correlation function [21,22]. A cutoff energy of 500 eV was employed for the plane wave basis set and the geometry optimizations were converged to a force cutoff of 0.01 eV/Å.

3. Results and discussion

3.1. Morphological characterizations

The morphology of the active material directly influences the performance and stability of the supercapacitor. The FE-SEM image of the as-synthesized FeS_2, which is composed of well-dispersed spheres with average diameter of about 1.3 μm as depicted in Fig. 1A. The high resolution FE-SEM image is shown in Fig. 1B, which confirms that the surface of spheres is composed of

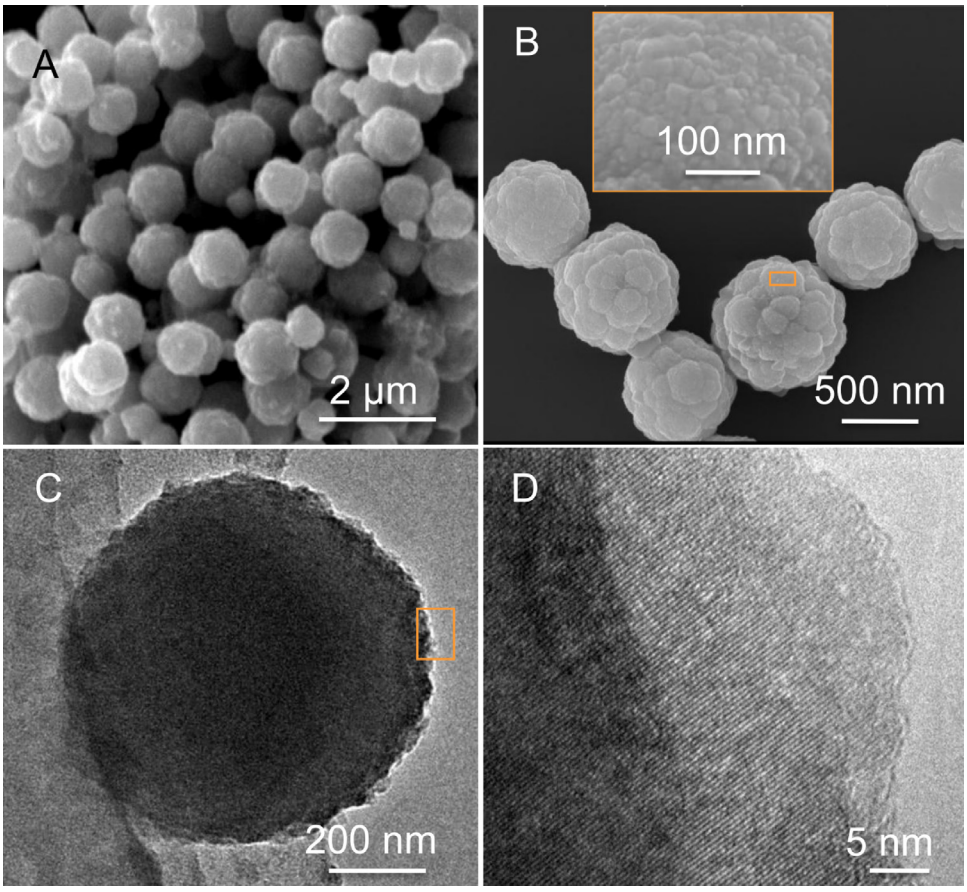

Fig. 1. FE-SEM and TEM images of the synthesized FeS_2 nanospheres (A) low resolution (B) high resolution FE-SEM image (Inset is the magnified part circled in B), (C) low resolution and (D) high resolution TEM images.

numerous compact packed nanoparticles with average size of 40–50 nm (inset in Fig. 1B). In addition, a large number of pores between these nanospheres and well-ordered nanoparticles with large surface area also provide the tunnels for efficient transportation of electrolyte ions to reach the reaction sites. The nano crystals would prevent deformation against strains and keep good stability during the charge storage process. From the TEM images (Fig. 1C), the spheres are solid in nature and from the edge of spheres, it is clear that the spheres are composed by nanoparticles which are in agreement with the high resolution FE-SEM observation. Such nanostructured aggregation provides high specific surface area which is beneficial for energy storages devices. To further investigate the structural details of the spheres, high resolution TEM (HR-TEM) was employed and the image of the selected edge portion of the spheres is shown in Fig. 1D, which indicates that the basic building blocks for the spheres are nanoparticles. Therefore, the nanoparticle aggregation spheres with tunnel structures are more effective for redox reactions in pseudocapacitive charge storage process. The high specific surface area of the FeS_2 spheres is 50.60 $m^2 g^{-1}$ calculated from BET result, which is higher than those of TMC's based supercapacitor electrode materials, such as zinc sulfide nanospheres (ZnS, 28 $m^2 g^{-1}$) [11], molybdenum disulfide nanospheres (MoS_2, 35 $m^2 g^{-1}$) [13] and cupper sulfide nanowires (Cu_7S_4, 34.23 $m^2 g^{-1}$) [4]. The The N_2 absorption and desorption isotherms and pore size distribution derived from desorption isotherm for FeS_2 spheres and are shown in Fig. S2A and B, which demonstrates that the average pore size is about 18 nm. Such a narrow pore size distribution is favorable for deep penetration of electrolyte ions and beneficial for efficient insertion/extraction of electrolyte ions during the charging/discharging process [23,24].

3.2. Electrochemical performance of FeS_2-nanosphers based supercapacitors

The electrochemical performance of the FeS_2-CP solid-state supercapacitor was first investigated using CV and GCD tests. The CV curves of the FeS_2-CP supercapacitor at various scan rates ranging from 5 to 150 m Vs^{-1} in the potential window of −0.8 to 0.8 V is depicted in Fig. 2A. The CP serves as a substrate and the straight line-like CV curve of pure CP based supercapacitor suggests that the substrate hardly contribute to the capacitance of the supercapacitor electrode as shown in Fig. S3. By increasing the scan rate the shape of CV curves remain the same even at higher scan rate of 150 m Vs^{-1}, which demonstrates that the FeS_2 electrodes possess excellent rate capability and good capacitive behavior. The large current response in the CV curves demonstrates the outstanding charge storage capability and rapid electrolyte ion transportation of the FeS_2 electrodes [25]. It is clear that the CV curves at various scan rates ranging from 50 to 150 mV s^{-1} have almost symmetrical shapes versus the zero current line and the current response increases with increasing the scan rates, which indicates that the adsorption and desorption of electrolyte ions occur on the inner surface of the active material in the electrode. GCD profiles of the FeS_2-CP supercapacitor in potential window of 0.0-0.8 V at various current densities 0.1-0.7 mA cm^{-2} are presents in Fig. 2B. The liner shape of charging/discharging cycles exhibits the excellent capacitive performance.

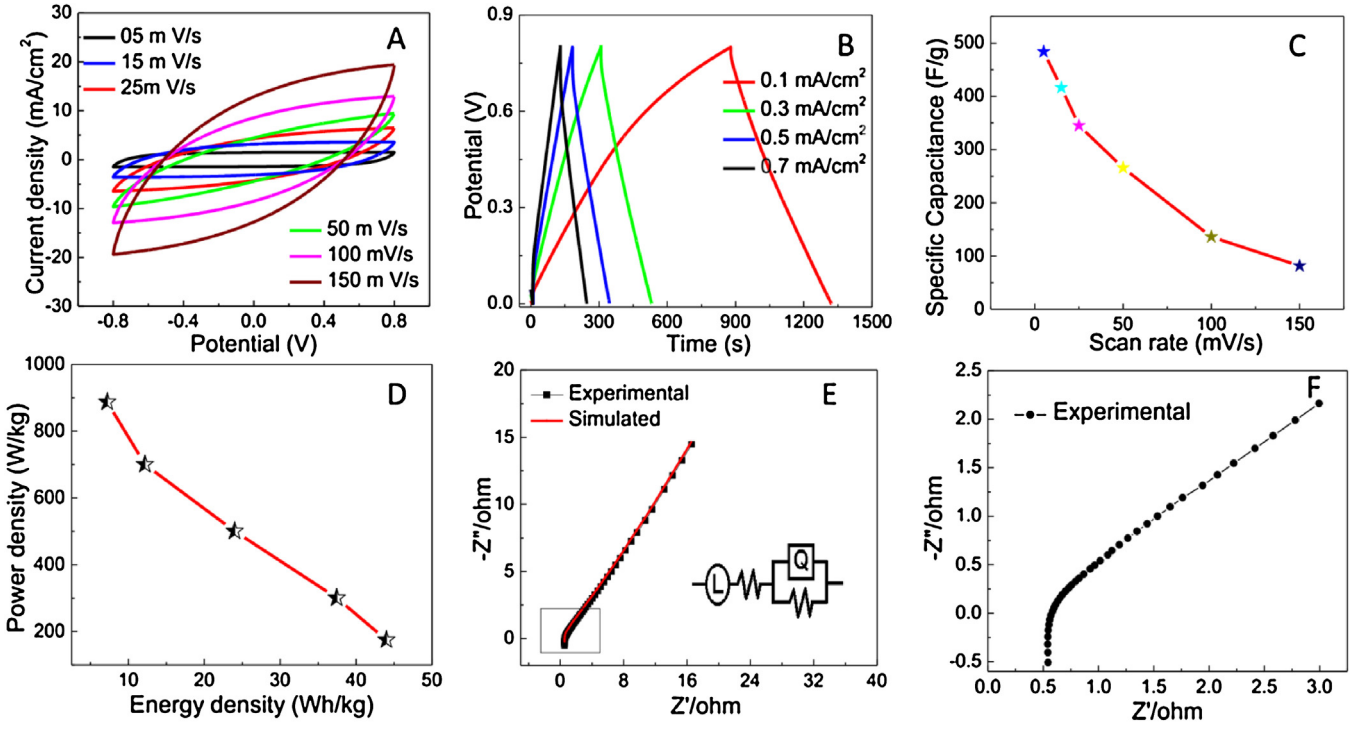

Fig. 2. Electrochemical performances of the FeS_2-CP solid state supercapacitor (A) CV curves at different scan rates ranging from 5 to 150 m Vs^{-1} in potential window of −0.8 to 0.8 V, (B) charging-discharging curves taken at different current densities ranging from 0.1 to 0.7 mA/cm^2 in potential window of 0 to 0.8 V, (C) specific capacitance as a function of scan rate, (D) Ragone plots (Energy density vs. Power density) of the supercapacitor. (E) Nyquist plot of impedance from 0.01 to 100 kHz, (Insets are the corresponding equivalent electrical circuit) and (F) enlarged high frequency part, circled in E.

The discharge curves at low current densities demonstrate the low *IR* drop, indicating that the FeS_2 nanospheres have good electrical conductivity and excellent electrode material for supercapacitors. The symmetry of the GCD curves at high current densities and the linear slope of the discharge current indicate the excellent capacitive behaviors [26].

The specific capacitance C_{sp} and areal capacitance C_{arl} are calculated from area under CV curves according to the Eqn1-2 (calculation details are found in the Supporting Information) [4,11,13]. The specific capacitances are 484, 416, 345.3 and 265 F g^{-1} at the scan rate of 5, 15, 25 and 50 m Vs^{-1} respectively, and are shown in Fig. 2C. The high areal capacitance of 135.5 and 28 mF cm^{-2} at scan rate of 5 and 200 m Vs^{-1} respectively, is achieved with a little high mass loading (1.8 mg cm^{-2}). The specific capacitance of FeS_2 nanospheres is higher than of previous reported symmetric supercapacitors based on TMC's (Table 1). Excellent electrochemical performance of the FeS_2-CP supercapacitor is attributed to the nanoparticle aggregated spheres resulted in multiple channels and high specific surface area for easy accessibility of electrolyte ions. To investigate the overall performance of the supercapacitor, the power density vs. Energy density (Ragone plots) for the FeS_2-CP supercapacitor is calculated and shown in Fig. 3D. A maximum energy density of 44 Wh kg^{-1} at high power density of 175 W kg^{-1} is obtained. The FeS_2-CP supercapacitor exhibits greater energy density and power densities than those of the previously reported symmetric supercapacitors based on iron oxide and TMCs. The detailed comparison of the current work with recent literatures is carried out and demonstrated in Table 1. As can be seen from Table 1, FeS_2 based single electrode and all solid state supercapacitor show higher

Table 1
The comparison of the FeS_2-CP based on three electrode system and symmetric full solid state supercapacitor with previous literatures, where we denote C_{SS} for Specific Capacitance (Three electrode system), C_{ST} for Specific Capacitance (two-electrode supercapacitor device), *E* for Energy density, *P* for Power and density and *n* for cycle numbers.

No	Materials	C_{SS} (F g^{-1})	C_{ST} (F g^{-1})	*E* (Wh kg^{-1})	*P* (W kg^{-1})	Stability (%) after *n*	Ref.
0	FeS_2 nanospheres	852.3 at 10 m Vs^{-1}	484 at 5 m Vs^{-1}	44	175	95.7, 5000	This work
1	Cu_7S_4 Nanowires	–	400 at 10 m Vs^{-1}	35	200	95, 5000	[4]
2	Co_9S_8 Nanoflakes	–	82.9 at 1 A g^{-1}	31.4	200	90, 5000	[10]
3	MoS_2 Nanospheres	–	368 at 5 m Vs^{-1}	5.42	128	96.5, 5000	[13]
4	KCu_4Se_8/V_2O_5 Nanowires	–	93.7 at 5 m Vs^{-1}	1.7	8.3	37.4, 5000	[31]
5	$NiMoO_4.xH_2O$	–	96.7 at 5 mA cm^{-2}	34.4	165	80.6, 1000	[32]
6	$FeCo_2O_4$ nanostructures	428 at 5 m Vs^{-1}	74 at 0.28 A g^{-1}	23	236	97, 1500	[33]
7	CoHCFe[a]	250 at 5 m Vs^{-1}	190 at 5 m Vs^{-1}	34.4	2.5k	88.9, 4000	[34]
8	$ZnFe_2O_4$	131 at 0.1 A g^{-1}	–	–	–	92, 1000	[35]
9	Fe_3O_4 nanoparticles	65.4 at 0.4 A g^{-1}	–	–	–	82, 3000	[36]
10	Fe_3O_4/rGO[b]	220.1 at 0.5 A g^{-1}	–	–	–	100, 3000	[36]
11	Fe_3O_4/rGO composites	154.5 at 10 m Vs^{-1}	–	–	–	60, 10000	[37]
13	Fe_3O_4–carbon nanosheets	163.4 at 1 A g^{-1}	–	–	–	93, 5000	[38]

[a] CoHCFe: Cobalt Hexacyanoferrate.
[b] rGO: Reduced graphene oxide.

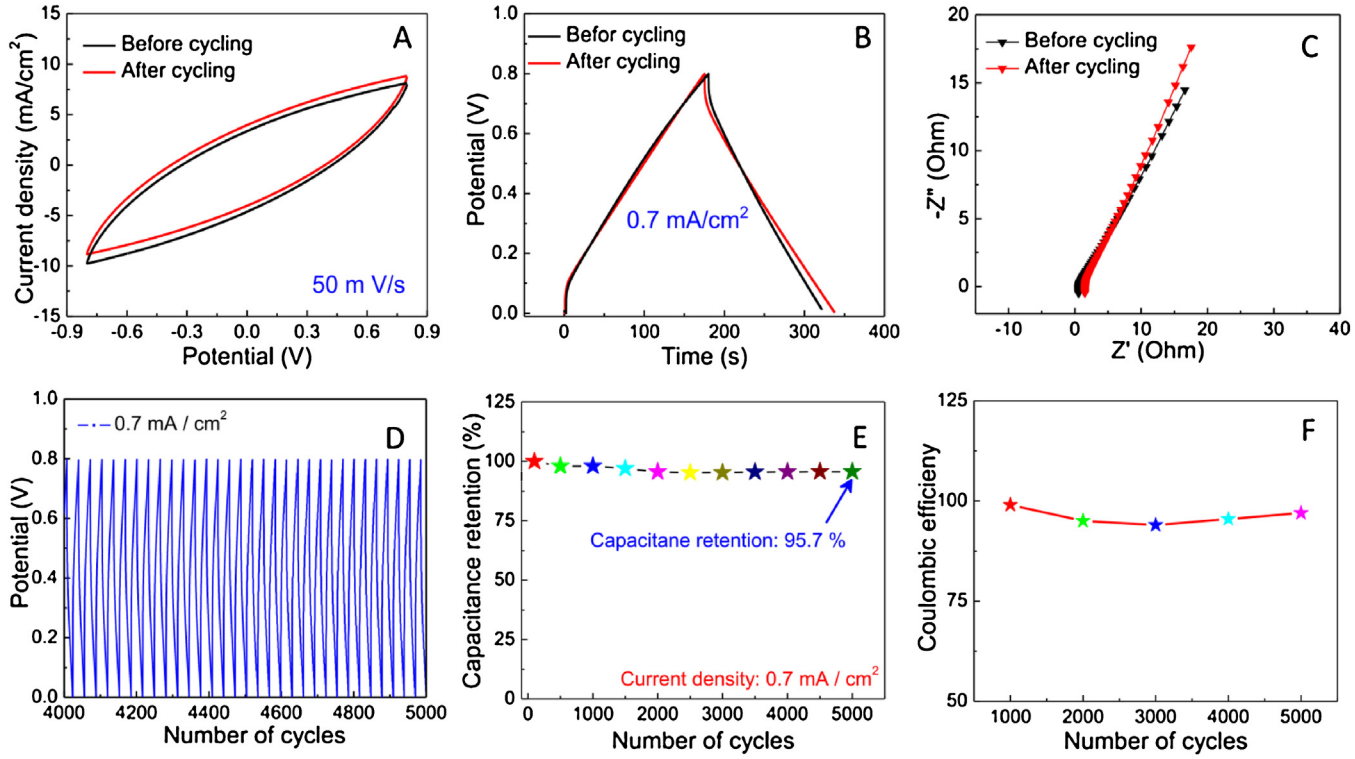

Fig. 3. Long term cycling performance of FeS_2-CP solid state supercapacitor, (A) CV curves before and after 5000 cycles at scan rate of 50 m Vs^{-1}, (B) charging-discharging curves before and after cycling process, taken at current density of 0.7 mA/cm^2, (C) EIS spectra before and after cycling process, (D) charging-discharging curves in potential window of 0 to 0.8 V taken at current density of 0.7 mA/cm^2 and (E) capacitance retention vs. number of cycles and (F) coulombic efficiency of supercapacitor vs. number of cycles.

specific capacitance than single iron oxides, composite of iron/graphene, binary oxides of iron and TMCs. The experimental results evidently show the FeS_2 is a promising electrode material for supercapacitors.

An insight into the capacitive and resistive behaviors of the FeS_2-CP based supercapacitor can be acquired from electrochemical impedance spectroscopy (EIS) analysis and the resultant Nyquist plot is shown in Fig. 2E, where the inset shows the equivalent circuit obtained by fitting the EIS spectrum using ZSimp Win impedance software. From the enlarged part of Nyquist plot, (Fig. 2F) the internal resistance (R_s) of the electrode material can be calculated from x-intercept at the high frequency range. The internal resistance includes the inherent resistance, contact resistance of the electrode material with substrate and ionic resistance of the electrolyte. From Fig. 2F, the value of R_s is 0.54 Ω, such small R_s can be attributed to the excellent electrical conductivity and easy ion accessibility of the FeS_2 nanospheres. Normally, EIS spectrum shows the semicircle presented by a parallel combination of internal capacitance and resistance of the material. In our case, the absence of the semicircle indicates the excellent contact between the active material (FeS_2) and CP [27].

The effect of scanning rates and potential windows has been investigated and results are presented in Fig. S4A and B, which indicates that the CV cycles of the FeS_2-CP supercapacitor have stable performance at various scan rates ranging from 10-100 mVs^{-1} and at different potential windows ranging from of −0.8-0.8 V. The GCD curves at the different current densities ranging from 0.2 to 0.8 mA cm^{-2} in potential window of 0.0 to 0.5 V reveal the existence of small potential drops (*IR* drop) of 0.037 V at 0.6 mA cm^{-2}, 0.023 V at 0.4 mA cm^{-2} and 0.011 V at 0.2 mA cm^{-2} as shown in Fig. S4C. The low *IR* drop indicates the quick *I–V* response and low internal resistance of the FeS_2-CP electrodes. The GCD cycles followed the same charging path to charge the supercapacitor for different potential windows from 0.2 to 1.0 V at constant current density of 0.5 mA cm^{-2}, demonstrates the stable charge storage characteristics in different voltage windows (Fig. S4D) [28,29].

Long life span is the most important factor in supercapacitor applications; we have compared the CV, GCD and EIS tests before and after completing the 5000 cycles, and the results are presented in Fig. 3A–C, respectively. The FeS_2-CP supercapacitor demonstrates the excellent stability and performance after long term cycling. It is observed that the performance of the supercapacitor after cycling become better, which is attributed to the full activation of electrode material and more pore opens during the insertion and extraction of the electrolyte ions throughout the active material, resulting in the more sites are activated for electrochemical reactions [30,31]. The cycling performance and the specific capacitance verses charge–discharge cycles are shown in Fig. 3D and E, respectively. From beginning to 1500 cycles the specific capacitance decreases and after that increases for next 500 cycles and then remains constant till 4000 cycles and finally increases up to 5000 cycles. The supercapacitor shows the excellent performance by retaining 95.7% of the initial capacitance after long term running of 5000 cycles (Fig. 3E). The stability of the supercapacitor was also investigated by calculating coulombic efficiency (η) at constant current density of 0.7 mA cm^{-2} and the results are shown in Fig. 3F. The η decreases from 100 to 94% in first 2900 cycles, then it keeps increasing up to 5000 cycles and attain the highest value of 97%.

The flexibility of FeS_2-CP supercapacitor was also checked by conducting electrochemical performance tests at different bending states. The CV and GDC curves were recorded at constant scan rate of 50 m Vs^{-1} and constant current density of 0.6 mA cm^{-2} at various bending angles (0°, 45°, 90° and 180°) as demonstrated in Fig. 4A and B, respectively. There is no obvious change observed in

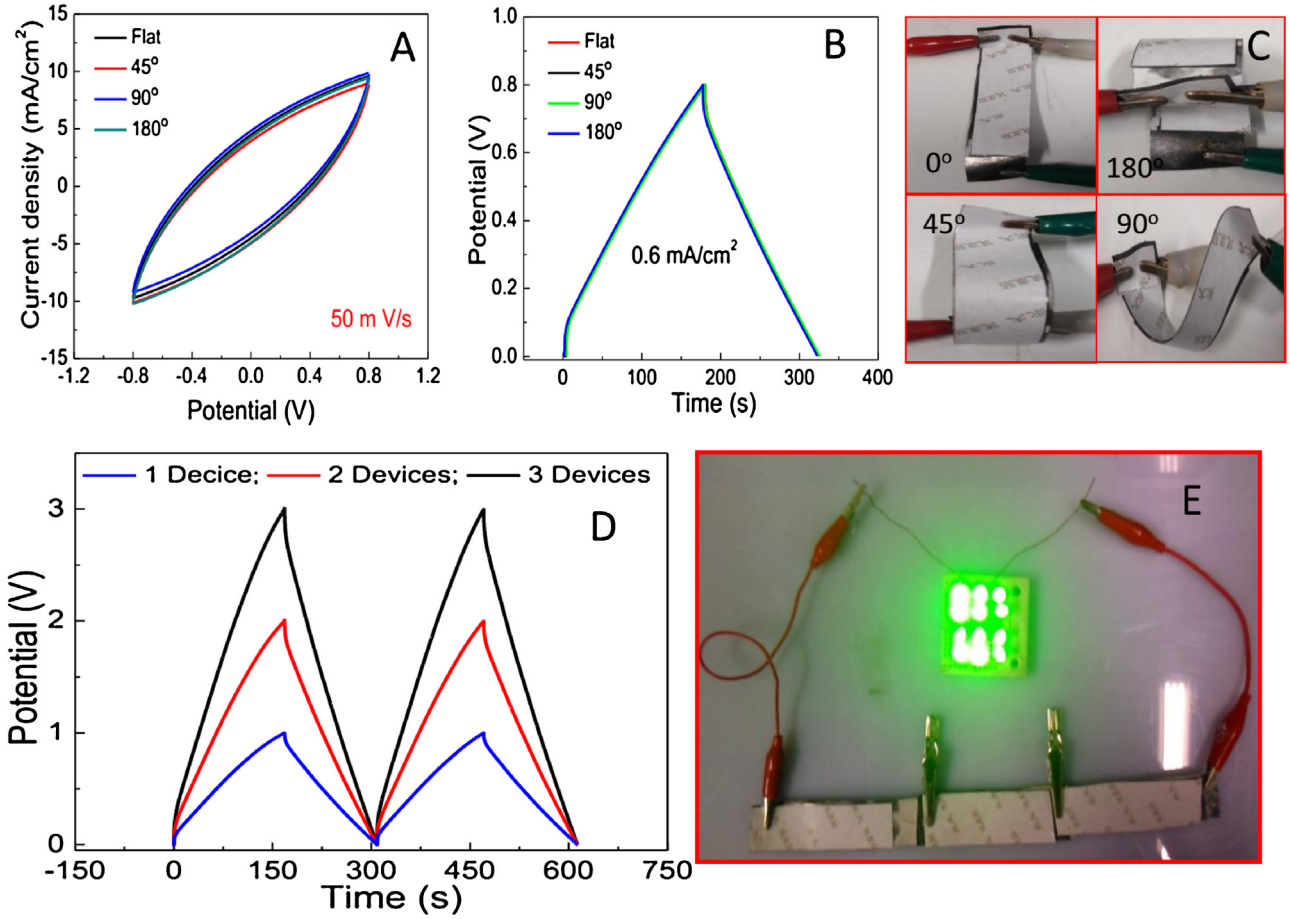

Fig. 4. Flexible performance of FeS_2-CP solid-state supercapacitor at different bending angles, the bent device has no effect on its performance as seen in (A) CV curves at a scan rate of 50 m Vs^{-1}, (B) charging-discharging curves taken at 0.6 mA/cm^2, (C) digital photographs of solid state supercapacitor bent at different angles showing the flexibility of the device, (D) Charging-discharging curves of FeS_2-CP supercapacitor at constant current density of 0.5 mA/cm^2, single device can charge up to 1 V, two devices in series can charge up to 2 V and three devices in series can charge up 3 V and (E) Three charged supercapacitors connected in series could light the 12 green-color LEDs brightly for 5.5 min. (For interpretation of the references to colour in this figure legend, the reader is referred to the web version of this article.)

CV and GDC curves, which demonstrates the same performance under different bending conditions and reveal good flexibility and stability of the supercapacitor [23]. The optical photographs of the FeS_2-CP supercapacitor under different bending states are shown in Fig. 4C.

To demonstrate practical applications, the charging-discharging curves of the three supercapacitors connected in series are recorded at constant current density of 0.5 mA cm^{-2} as is shown in Fig. 4D. Single SC, two and three SCs connected in series can be charged up to 1 V, 2 V and 3 V, respectively. Three charged SCs in series are able to light 12 green-color, commercial LEDs (5 mm diameter, 3.0 V, 20 mA) for 5.5 minutes, the digital photograph and video are shown in Fig. 4E and Video 1 (see video in the Supporting Information), respectively.

To check the pseudocapacitive behavior of FeS_2-nanosphers electrode, we carried out CV and GCD tests in 1 M LiCl aqueous electrolyte in three-electrode system. The representative CV curves recorded at various scan rates ranging from 10 to 200 m Vs^{-1} in potential window of −0.4 to 0.8 V is depicted in Fig. 5A. CV curves indicate the pseudocapacitive behavior with a pair of well-defined redox peaks. The CV curves of pristine CP and FeS_2-CP are presented in Fig. S5, indicating that the contribution from the pristine CP based electrode is negligible. It is observed that the peak currents increase with the increasing scan rates which demonstrate that FeS_2-nanospheres possess excellent capacitive features [24].

The specific capacitance (C_{sp}) for single electrode is calculated from CV curves [4,11,13] according to the equation (1) (calculation details are found in the Supporting Information). The specific capacitance of 852.3, 746, 631 and 496 F g^{-1} at the scan rate of 10, 25, 50 and 75 m Vs^{-1} is achieved, respectively. The specific capacitance as a function of scan rate is illustrated in Fig. 5B. The C_{sp} of FeS_2-nanospheres based electrode still retains at 269.5 F g^{-1} at high scan rate of 200 m Vs^{-1} demonstrating the good rate capability, such good pseudocapacitive performance for metal chalcogenides is rarely reported. Fig. 5C shows the GCD curves for the FeS_2 nanospheres electrode at different current densities in potential window of 0.0 to 0.5 V. The pseudocapacitve features is also confirmed from GCD curves at different current densities [25]. The electrochemical performance of the electrode is further confirmed from a long term cycling test at constant current density of 8 A g^{-1} as is shown in Fig. 5D. After 1000 cycles the electrode shows a negligible loss (1.5%) as compared to the initial specific capacitance. The CV curves in the three-electrode system are obviously different from the two-electrode system (no redox peaks). The FeS_2-CP supercapacitor is charged and discharged at a pseudo-constant rate over the entire voltammetric cycles, which means that the continuous redox reactions are proceeds on the surface/inside of the electrode material. This is a common phenomenon observed in many symmetric supercapacitors reported in literature [11,16,27].

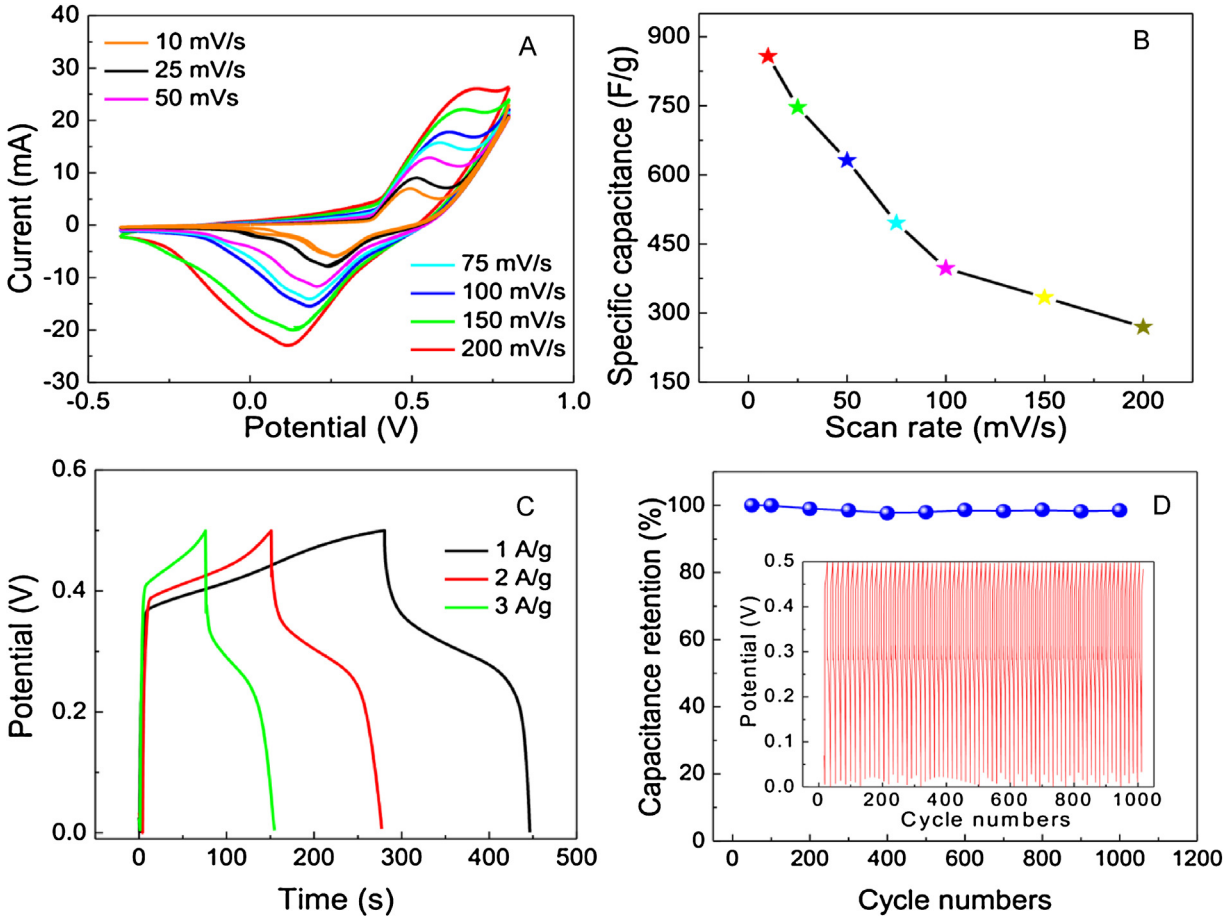

Fig. 5. Electrochemical performances of the FeS_2 nanospheres electrode in 1 M of LiCl aqueous electrolyte (A) CV curves at different scan rates ranging from 10 to 200 m Vs^{-1} in potential window of −0.5 to 1 V, (B) The specific capacitance as a function of scan rate, (C) charging-discharging curves taken at different current densities from 1 to 3 A/g in potential window of 0 to 0.5 V and (D) capacitance retention of FeS_2 nanospheres electrode verses number of cycles, (Inset, cycling performance of FeS_2 nanospheres electrode at constant current density of 5 A/g).

To further understand the supercapacitive behaviors from the crystal structure, the X-ray powder diffraction pattern of the synthesized FeS_2 is shown in Fig. 6A. All diffraction peaks are indexed to the orthorhombic crystal structure with a = 4.445 Å, b = 5.425 Å and c = 3.388 Å according to the standard JCPDS card No: 65-2567. The space group of FeS_2 crystal structure is Pnnm [58], in which the one Fe atom is surrounded by 6 S atoms to form FeS_6 octahedron. S atoms are located at the apexes and Fe atom is in the center of the octahedron. The octahedrons stack on each other periodically and tunnels are formed along c direction as shown in Fig. 6B. The lattice parameters are analyzed during charging and discharging process as depicted in Fig. 6C, which can be seen that lattice parameters significantly change with the amount of intercalated lithium ions. As the stacking of octahedrons is anisotropic, the lattice parameters change anisotropically, where a-axis is the most enlarged direction. Such expansion in volume significantly increase the space of the tunnels. Based on the symmetry structure of FeS_2 and minimum distance between Li sites, there is only one potential path for Li hopping (Fig. 6D). The path requires Li hopping between two neighboring center of S8 octahedron along the c axis. Li ions hops from one S8 octahedron center to the other through inside of a pyramid as shown in Fig. 6D–E. The diffusion path of Li in FeS_2 structure are calculated, where x-axis is the distance along the path between Li in the initial and final states. Since the size of the diffusion tunnels changes with the amount the lithium ions, the energy barrier for a diffusing lithium ion also reduces with it. We have calculated the lithium-rich FeS_2, where the barrier is lower than 0.5 eV, as shown in Fig. 6F. We have also calculated the diffusion coefficient can be expressed as $D = g\,l^2\,\Gamma$, where Γ is hopping frequency from filled to vacant site, and g is a geometric factor relating to the number of nearest neighbors and the lattice topology (in this work, $g = 1$). According to the transition state theory, Γ can be expressed as $\Gamma = \nu^* \exp(-E_a/K_B T)$, where ν^* is the attempt frequency (within the range of phonon frequency, about 10^{13} Hz. Considering the diffusion coefficient within the range of 10^{-13} *to* 10^{-7} $(cm^2\,s^{-1})$, the diffusion coefficient of the path can be approximated to be 4.5×10^{-11} $(cm^{-2}\,s^{-1})$, which indicates that it is relatively favorable for Li ions diffusion along this path. In addition, the discharge curve versus lithium for FeS_2 supercell is shown in Fig. S6. The network structures of the octahedrons provide proper tunnels, which could give the diffusion path for the ion intercalation/de-intercalation during the charging/discharging process. Therefore, FeS_2 could be good electrode material for supercapacitor due to the network and tunnel structure.

On the whole, the improvement in energy and power densities of the FeS_2-CP supercapacitor is effected by the following points: (1) FeS_2 has tunnel-structure, beneficial to insertion/extraction of Li^+ ions. (2) The nanoparticle aggregated spheres offers larger interfacial area which accommodates deformation by the ion insertion. (3) The open space between nanospheres allows easy diffusion of electrolyte ions into the inner region of the active material and CP provides good conductivity. These results

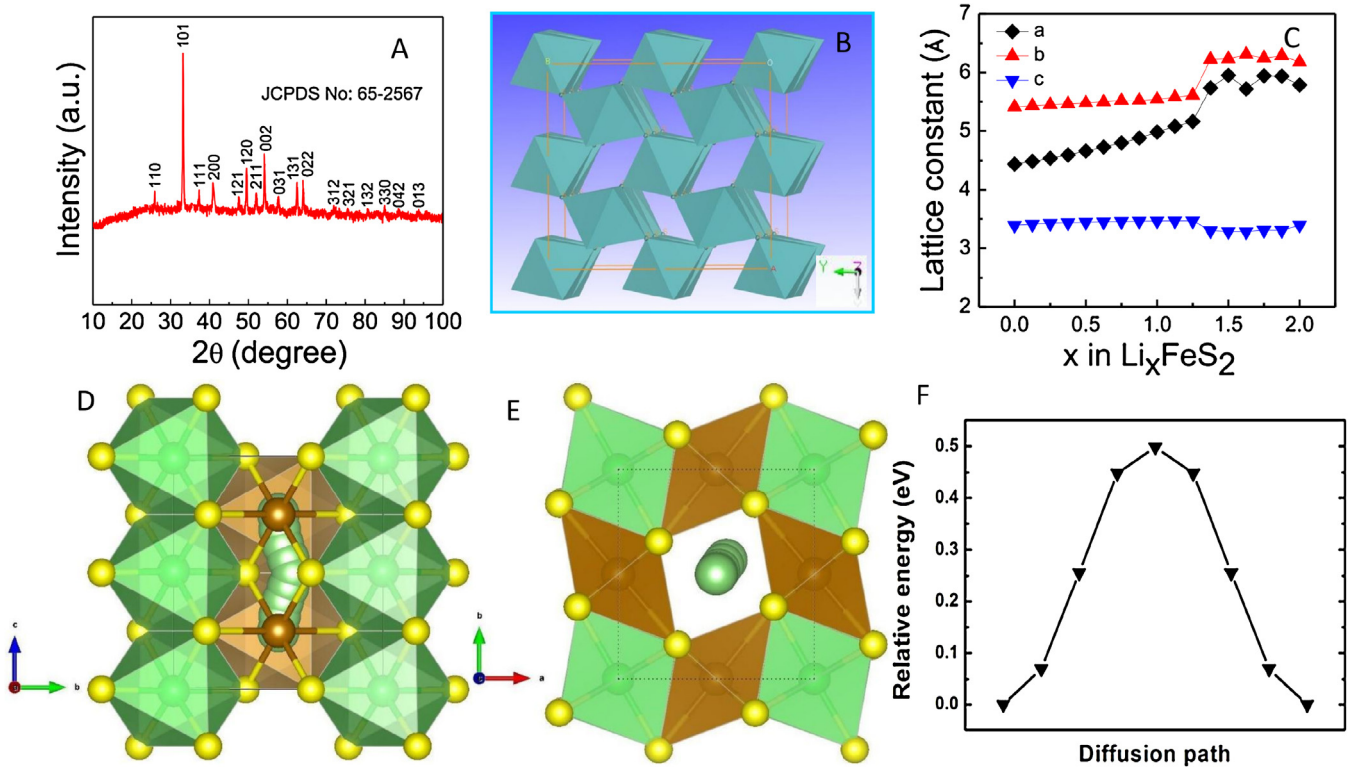

Fig. 6. (A) XRD pattern of synthesized FeS_2 nanospheres, (B) Orthorhombic crystal structure of FeS_2 with tunnels, (C) Variation of lattice constants during charge-discharge process (D) and (E) Li ion diffusion path in tunnels of lithium-rich FeS_2 along c direction. (Li is green balls, Fe is inside brown tetrahedrons and S is yellow balls, insides the green balls are the intercalated lithium ions, the caterpillar-like green pillar is the combined NEB images, which compose the diffusion path.) and (F) Relative energy vs. diffusion path for the diffusion of Li^+ ions. (For interpretation of the references to colour in this figure legend, the reader is referred to the web version of this article.)

demonstrate that the FeS_2-CP supercapacitor is promising candidate for applications in high performance energy storage devices.

4. Conclusion

In summary, FeS_2 nanospheres have been synthesized by cost effective hydrothermal method. The nanospheres are aggregated by small nanocrystals, which offer large specific area and ion diffusion channels to enhance the active sites. The supercapacitive behaviors of the FeS_2 nanospheres are investigated in details through a single electrode in the liquid electrolyte and two symmetric electrodes in the solid state electrolyte. The FeS_2 nanospheres possess network structure of FeS_6 octahedrons, which forms tunnels along its c-axis. The tunnels provide diffusion paths for the ion intercalation/de-intercalation during the charging/discharging process. A symmetrical solid-state flexible supercapacitor based on FeS_2 nanospheres supported on the carbon paper exhibits a high specific capacitance (484 $F g^{-1}$, 5 m Vs^{-1}), excellent rate capability and cycling ability by retaining the 95.7% capacitance after 5000 charge/discharge cycles. A maximum energy density of 44 Wh kg^{-1} at a power density of 175 W kg^{-1} is achieved with 97% coulombic efficiency. Furthermore, three charged supercapacitor connected in series can power 12 green-color commercial LEDs (3.0 V, 20 mA) effectively for 5.5 min. The impressive performance of the FeS_2-CP supercapacitor suggests that the FeS_2 sphere assembled by nanoparticles is a promising electrode material for supercapacitors.

Acknowledgments

This work is supported by NSFC (51572040), Chongqing University Postgraduates' Innovation Project (CYB15044), National High Technology Research and Development Program of China (2015AA034801), NSFCQ (cstc2015jcyjA20020), The Science and Technology Research Project of Chongqing Municipal Education Commission of China (KJ130603,KJKJ1400607).

Appendix A. Supplementary data

Supplementary data associated with this article can be found, in the online version, at http://dx.doi.org/10.1016/j.electacta.2016.10.060.

References

[1] A. Yu, V. Chabot, J. Zhang, Electrochemical supercapacitors for energy storage and delivery: fundamentals and applications, CRC Press, 2013.
[2] P. Yang, W. Mai, Nano Energy 8 (2014) 274–290.
[3] K. Zhou, W. Zhou, L. Yang, J. Lu, S. Cheng, W. Mai, Z. Tang, L. Li, S. Chen, Adv. Fun. Mater. 25 (2015) 7530–7538.
[4] M.S. Javed, S. Dai, M. Wang, Y. Xi, Q. Lang, D. Guo, C. Hu, Nanoscale 7 (2015) 13610–13618.
[5] P. Yang, X. Xiao, Y. Li, Y. Ding, P. Qiang, X. Tan, W. Mai, Z. Lin, W. Wu, T. Li, ACS nano 7 (2013) 2617–2626.
[6] M.R. Gao, Y.F. Xu, J. Jiang, S.H. Yu, Chem. Soc. Rev. 42 (2013) 2986–3017.
[7] X. Li, C. Hu, X. Kang, Q. Len, Y. Xi, K. Zhang, H. Liu, J. Mater. Chem. A 1 (2013) 13721–13726.
[8] K. Zhang, Y. Xi, C. Hu, Sci. Adv. Mater. 7 (2015) 2206–2215.
[9] J.A. Wilson, J. Phy. Cond. Matt. 22 (2010) 203201.
[10] W. Zhou, X. Cao, Z. Zeng, W. Shi, Y. Zhu, Q. Yan, H. Liu, J. Wang, H. Zhang, Energy Environ. Sci. 6 (2013) 2216–2221.
[11] M.S. Javed, J. Chen, L. Chen, Y. Xi, C. Zhang, B. Wan, C. Hu, J. Mater. Chem. A 4 (2016) 667–674.
[12] H. Wan, X. Ji, J. Jiang, J. Yu, L. Miao, L. Zhang, S. Bie, H. Chen, Y. Ruan, J. Power Sources 243 (2013) 396–402.
[13] M.S. Javed, S. Dai, M. Wang, D. Guo, L. Chen, X. Wang, C. Hu, Y. Xi, J. Power Sources 285 (2015) 63–69.
[14] M. Sun, J. Tie, G. Cheng, T. Lin, S. Peng, F. Deng, F. Ye, L. Yu, J. Mater. Chem. A 3 (2015) 1730–1736.
[15] S. Dai, Y. Xi, C. Hu, X. Yue, L. Cheng, G. Wang, J. Power Sources 263 (2014) 175–180.

[16] W. Hu, R. Chen, W. Xie, L. Zou, N. Qin, D. Bao, ACS App. Mater. Inter. 6 (2014) 19318–19326.
[17] S. Dai, Y. Xi, C. Hu, J. Liu, K. Zhang, X. Yue, L. Cheng, J. Mater. Chem. A 1 (2013) 15530–15534.
[18] S. Devaraj, N. Munichandraiah, The J. Phy. Chem. C 112 (2008) 4406–4417.
[19] R. Dong, Q. Ye, L. Kuang, X. Lu, Y. Zhang, X. Zhang, G. Tan, Y. Wen, F. Wang, ACS App. Mater. Inter. 5 (2013) 9508–9516.
[20] D. Rickard, G.W. Luther, Chem. Rev. 107 (2007) 514–562.
[21] J.P. Perdew, K. Burke, M. Ernzerhof, Phys. Rev. Lett. 77 (1996) 3865.
[22] M.S. Javed, X. Han, C. Hu, M. Zhou, Z. Huang, X. Tang, X. Gu, ACS App. Mater. Inter. 8 (2016) 24621–24628.
[23] G. Henkelman, H. Jónsson, J. Chem. Phys. 113 (2000) 9978–9985.
[24] M.S. Javed, C. Zhang, L. Chen, Y. Xi, C. Hu, J. Mater. Chem. A 4 (2016) 8851–8859.
[25] S. Zhao, T. Liu, M.S. Javed, W. Zeng, S. Hussain, Y. Zhang, X. Peng, Electrochim. Acta 191 (2016) 716–723.
[26] P. Hao, Z. Zhao, J. Tian, H. Li, Y. Sang, G. Yu, H. Cai, H. Liu, C. Wong, A. Umar, Nanoscale 6 (2014) 12120–12129.
[27] B. Liu, B. Liu, Q. Wang, X. Wang, Q. Xiang, D. Chen, G. Shen, ACS App. Mater. Inter. 5 (2013) 10011–10017.
[28] Z. Hu, X. Xiao, C. Chen, T. Li, L. Huang, C. Zhang, J. Su, L. Miao, J. Jiang, Y. Zhang, Nano Energy 11 (2015) 226–234.
[29] M. Yang, H. Cheng, Y. Gu, Z. Sun, J. Hu, L. Cao, F. Lv, M. Li, W. Wang, Z. Wang, Nano Res. 8 (2015) 2744–2754.F.
[30] W. Zhou, X. Liu, Y. Sang, Z. Zhao, K. Zhou, H. Liu, S. Chen, ACS App. Mater. Inter. 6 (2014) 4578–4586.
[31] K. Zhang, H. Chen, X. Wang, D. Guo, C. Hu, S. Wang, J. Sun, Q. Leng, J. Power Sources 268 (2014) 522–532.
[32] M.-C. Liu, L. Kang, L.-B. Kong, C. Lu, X.-J. Ma, X.-M. Li, Y.-C. Luo, RSC Adv. 3 (2013) 6472–6478.
[33] A. Pendashteh, J. Palma, M. Anderson, R. Marcilla, J. Mater. Chem. A 3 (2015) 16849–16859.
[34] F. Zhao, Y. Wang, X. Xu, Y. Liu, R. Song, G. Lu, Y. Li, ACS App. Mater. Inter. 6 (2014) 11007–11012.
[35] M. Zhu, X. Zhang, Y. Zhou, C. Zhuo, J. Huang, S. Li, RSC Adv. 5 (2015) 39270–39277.
[36] T. Qi, J. Jiang, H. Chen, H. Wan, L. Miao, L. Zhang, Electrochim. Acta 114 (2013) 674–680.
[37] D. Guan, Z. Gao, W. Yang, J. Wang, Y. Yuan, B. Wang, M. Zhang, L. Liu, Mater. Sci. Eng. B 178 (2013) 736–743.
[38] D. Liu, X. Wang, X. Wang, W. Tian, J. Liu, C. Zhi, D. He, Y. Bando, D. Golberg, J. Mater. Chem. A 1 (2013) 1952–1955.